CONDENSED MATTER PHYSICS

Correlation between unconventional superconductivity and strange metallicity revealed by operando superfluid density measurements

Ruozhou Zhang[1,2]†, Mingyang Qin[1,3]†*, Chenyuan Li[4]†, Zhanyi Zhao[1,5]†, Zhongxu Wei[1,6], Juan Xu[1], Xingyu Jiang[1,5], Wenxin Cheng[1,5], Qiuyan Shi[1,5], Xuewei Wang[1,5], Jie Yuan[1,5,7], Yangmu Li[1,5], Qihong Chen[1,5,7], Tao Xiang[1,8], Subir Sachdev[4]*, Zi-Xiang Li[1,5]*, Kui Jin[1,5,7]*, Zhongxian Zhao[1,5,7]

Strange-metal behavior has been observed in superconductors ranging from cuprates to pressurized nickelates, but its relationship to unconventional superconductivity remains elusive. Here, we perform operando superfluid density measurements on ion-gated FeSe films. We observe a synchronized evolution of the superconducting condensate and the strange-metal phase with electron doping, from which a linear scaling between zero-temperature superfluid density and strange-metal resistivity coefficient is further established. The scaling also applies to different iron-based and cuprate superconductors despite their distinct electronic structures and pairing symmetries. Such a correlation can be reproduced in a theoretical calculation on the two-dimensional Yukawa-Sachdev-Ye-Kitaev model by considering a cooperative effect of quantum critical fluctuation and disorder. These findings suggest that a common mechanism may govern both the Cooper pair condensation and the normal-state strange metallicity in unconventional superconductors.

INTRODUCTION

In the search for the microscopic mechanism of unconventional superconductors, a concerted effort has been directed toward understanding their normal states and how they link to superconductivity. It has been found that the normal state of various unconventional superconductors, e.g., cuprates (*1*–*3*), iron-based materials (*4*, *5*), magic-angle graphene (*6*), and nickelates (*7*–*9*) exhibits a linear-in-temperature (*T*-linear) resistivity extending to the low temperature. Such an anomalous transport behavior (*10*), termed as the strange metal, is acknowledged to be intimately related to unconventional superconductivity (*1*–*3*, *5*, *11*). However, despite extensive investigations over the past decades (*12*–*15*), the microscopic mechanism of strange-metal transport and the interplay between strange metal and superconductivity remain actively debated. One of the central questions is what the fundamental correlation between the strange-metal normal state and superconductivity is. To find clues for solving the puzzle, inspecting the crucial ingredient governing superconductivity across the strange-metal regime is immensely required.

One key parameter characterizing the superconducting state is the superfluid density, ρ_s ($\equiv \lambda_{ab}^{-2} \propto n_s / m*$, with λ_{ab} the in-plane magnetic penetration depth, n_s the superconducting carrier density, and $m*$ the effective electron mass), which encodes the phase rigidity of Cooper pairs, reflecting the resilience of pairing condensate against phase fluctuations. It has been widely observed in cuprates that the superconducting transition temperature (T_c) scales with ρ_{s0} [$\equiv \rho_s(T \to 0)$] [see, e.g.,(*16*–*20*)], which is beyond the standard Barden-Cooper-Schrieffer (BCS) scenario in which T_c is determined by the pairing strength (*16*, *17*, *21*). More intriguingly, in overdoped cuprates such as $Tl_2Ba_2CuO_{6+\delta}$ (Tl2201) and $La_{2-x}Sr_xCuO_4$ (LSCO), the normal-state carrier density increases with hole doping, but both ρ_{s0} and the *T*-linear resistivity coefficient A_1 decrease (*12*, *22*), suggesting a pivotal role of the strange-metal scattering in the pairing condensate. Consequently, establishing a quantitative relationship between ρ_{s0} and A_1 and exploring to what extent it can be applied to unconventional superconductors are of vital importance in understanding the essential physics underlying the connection between unconventional superconductivity and the strange metallicity and establishing a unified theoretical framework of unconventional superconductors. However, the great challenges involve manipulating superconductivity minutely across the strange-metal regime and obtaining precise ρ_{s0} data in an efficient way.

For LSCO, the systematic evolution of ρ_{s0} with T_c in the overdoped regime has been revealed by Božović *et al.* (*20*), based on data from more than 2000 films prepared over about 12 years. Other than chemical substitution methods, the ionic-liquid gating (ILG) technique is an approach that can continuously tune T_c of a single sample by virtue of either electrostatic or electrochemical effects (*23*). FeSe, a prototype iron-based superconductor with the simplest crystal structure containing only the Fe-Se layer, has shown its unique compatibility with the ILG technique, i.e., the almost fivefold enhancement of T_c under gating (*24*). The strange-metal state of FeSe films with *T*-linear resistivity, linear-in-field (*H*) magnetoresistance, and *H*/*T* scaling of magnetoresistance was unambiguously identified, and its evolution with ILG was also disclosed in our previous work (*5*).

Here, we perform operando ρ_s measurements by the two-coil mutual inductance (TCMI) technique on the ion-gated FeSe films, with

[1]Beijing National Laboratory for Condensed Matter Physics, Institute of Physics, Chinese Academy of Sciences, Beijing 100190, China. [2]State Key Laboratory of Surface Physics and Department of Physics, Fudan University, Shanghai 200433, China. [3]Department of Materials Science and Engineering, Southern University of Science and Technology, Shenzhen 518055, China. [4]Department of Physics, Harvard University, Cambridge, MA 02138, USA. [5]School of Physical Sciences, University of Chinese Academy of Sciences, Beijing 100049, China. [6]Department of Physics, Southern University of Science and Technology, Shenzhen 518055, China. [7]Songshan Lake Materials Laboratory, Dongguan, Guangdong 523808, China. [8]Beijing Academy of Quantum Information Sciences, Beijing 100193, China.
*Corresponding author. Email: qinmy@sustech.edu.cn (M.Q.); sachdev@g.harvard.edu (S.S.); zixiangli@iphy.ac.cn (Z.-X.L.); kuijin@iphy.ac.cn (K.J.)
†These authors contributed equally to this work.

T_c finely tuned in a wide range of ≈11 to 43 K in a single sample. With this high-efficiency approach, we uncover a systematic dependence of T_c on ρ_{s0} for the iron-based superconductors, i.e., $T_c \propto \rho_{s0}^{0.55\pm0.11}$. Intriguingly, we find that the superfluid condensate keeps in lockstep with the strange-metal phase during the gating process. A linear correlation between ρ_{s0} and A_1, i.e., $\rho_{s0} \sim A_1$, is further quantified, which also works for iron pnictides and overdoped cuprates. Such a relation is in good agreement with the calculations on the two-dimensional Yukawa-Sachdev-Ye-Kitaev (2D-YSYK) model (*25*–*27*), which describes fermions coupled to nearly critical bosonic modes with spatially disordered Yukawa interactions, taking into account the possible variation of quantum critical fluctuations and disorder strength during the gating or doping in experiments. Our findings reveal the quantitative connection between unconventional superconductivity and the strange metallicity, which may be common to the physics of different unconventional superconductors. (In this text, the symbols "∝" and "~" denote a proportional relationship and a generic linear relationship allowing for a constant intercept, respectively.)

RESULTS

Operando superfluid density measurements

FeSe films ($T_c \approx 11$ K) with thicknesses of 60 ± 5 nm were deposited on (001)-oriented LiF substrates with a size of 5 mm by 5 mm by the pulsed laser deposition technique. The x-ray diffraction measurements confirm the high-quality (00*l*) oriented growth of the film (Supplementary Text 1 and fig. S1). The pristine films were loaded in our ILG device as schematically shown in Fig. 1A. An ionic liquid *N*,*N*-diethyl-*N*-(2-methoxyethyl)-*N*-methyl ammonium bis(trifluoromethylsulfonyl) imide (DEME-TFSI) was used as the dielectric, covering both the FeSe film and the gate electrode. Under a positive gate voltage, the H^+ ions in the ionic liquid enter the FeSe film, which has been evidenced by the time-of-flight secondary ion mass spectroscopy (TOF-SIMS) measurements (*5*). Such an electron doping effect brings forth a transition in the carrier type of FeSe from the coexistence of electrons and holes to high-density electrons only (Supplementary Text 2 and fig. S3), which is accompanied by an enhancement of T_c to ≈40 K (*5*, *24*).

The superfluid density, $\rho_s \equiv \lambda_{ab}^{-2}$, is difficult to be accurately measured because λ_{ab} is typically thousands of angstroms. The TCMI technique is a suitable method to obtain the absolute value of ρ_s of superconducting films, which has attracted increasing attention due to its high sensitivity and flexibility (*20*). To in situ monitor the evolution of ρ_s of FeSe films, the ILG device was integrated into a homemade transmission-type TCMI apparatus (Materials and Methods and fig. S4) that consists of a drive coil and a pickup coil (*28*). Figure 1C shows the temperature-dependent real component of the pickup coil voltage, V_x, for the pristine state (red line) and the gated state with $T_c \approx 43$ K (blue line). The rapid drop in V_x around T_c originates from the diamagnetic effect of the screening supercurrent j_s. The spatial distribution of j_s is associated with the absolute value of ρ_s according to the self-consistent London equation (Materials and Methods). Using a self-developed fast wavelet collocation (FWC) method (*29*), we have solved the distributions of j_s for different ρ_s values (Fig. 1B) and then calculated the values of V_x by integrating the vector potential from the drive-coil current and j_s around each loop of the pickup coil. The absolute value of ρ_s can be accurately extracted by interpolating the measured V_x into the calculated V_x-ρ_s relation (Supplementary Text 3 and fig. S5), as shown in Fig. 1D.

By minutely tuning the superconductivity of the FeSe film via the ILG technique, a systematic evolution of V_x is obtained. It is shown that the diamagnetic signals exhibit a quasiparallel shift to high temperature with gating (Supplementary Text 4 and fig. S6). Each curve exhibits only a single transition (see also the inset of Fig. 1C, demonstrating the absence of the diamagnetic transition near the original T_c of 11 K), confirming the homogeneous modulation of the superconductivity by ILG (*28*). In other words, the H^+ ions have penetrated throughout the entire film thickness of 60 nm, consistent with their relatively large protonation length of up to 250 nm revealed by the TOF-SIMS measurements (*5*). Figure 2A shows the extracted temperature dependence of superfluid density, $\rho_s(T)$, for all gated states. A common feature is the flattening of ρ_s at low temperatures, which becomes more prominent for higher-T_c states. Such a feature has been observed in iron-based superconductors, e.g., $Ba_{1-x}K_xFe_2As_2$ (*30*), noted as an indication of the nodeless pairing gap. We fit the $\rho_s(T)$ data with a nodeless gap equation, i.e., $\rho_s(T) = \rho_{s0}\left(1 - Ce^{-\Delta_{min}/k_BT}\right)$, where Δ_{min} is the minimum gap size, k_B is the Boltzmann constant, C is the numerical parameter, and ρ_{s0} is the superfluid density at zero-temperature limit, which works well at low temperatures (see Fig. 2B). We note that the ρ_{s0} value of the pristine FeSe film (1.09 ± 0.09 μm^{-2}) is consistent with the value of $FeSe_{1-x}Te_x$ film (1.29 ± 0.11 μm^{-2}) measured by the scanning SQUID microscope (*31*) but is about 1/6 of the bulk FeSe [6.25 μm^{-2}; (*32*)]. Such a relatively low ratio of thin film to bulk crystal seems ubiquitous in unconventional superconductors, e.g., 1/5 for $Ba(Fe_{1-x}Co_x)_2As$ (*33*, *34*) and 1/9 for $YBa_2Cu_3O_{6+y}$ (*35*, *36*), which was attributed to the relatively strong quantum phase fluctuations (*37*) and/or disorder effect (*38*) in thin films.

Dependence of critical temperature on superfluid density

With the systematic ρ_s data, we explore the dependence of T_c on ρ_{s0}, which exhibits a simple power-law behavior (Fig. 2C), that is, $T_c = \gamma\rho_{s0}^{0.55\pm0.11}$, where γ is a numeric parameter. Here, the uncertainty in the power-law exponent is mainly caused by the error bars of the T_c value, i.e., ΔT_c, which may be associated with the strong superconducting fluctuations of FeSe (*32*). T_c and ΔT_c are the position and the full width at half maximum of the dip of V_y, respectively, following the definitions in (*35*). Such a relationship between T_c and ρ_{s0} holds well against different gap symmetries used to extract ρ_{s0} (Supplementary Text 5 and fig. S7). This study emphasizes the systematic $T_c(\rho_{s0})$ scaling established in iron-based superconductors, benefiting from our high-efficiency operando measurements.

It was suggested that a power-law index of ≈0.5 might occur in the dirty limit of a *d*-wave BCS superconductor (*39*, *40*). However, such a simple "dirty" BCS picture could not quantitatively explain our observations because our data unambiguously violate the Homes' law, i.e., $\rho_{s0} \propto \sigma_{dc}T_c$ (where σ_{dc} is the normal-state conductivity measured close to T_c) (fig. S8), that typically holds for a dirty BCS superconductor owing to the Glover-Ferrell-Tinkham sum rule (*20*, *41*, *42*). Notably, such a power-law behavior is in contrast to the linear relationship expected for a pure 2D superconductor without the effect of competing order and away from the superconducting quantum critical point (QCP) (*21*), suggesting that the $T_c(\rho_{s0})$ scaling in actual thin films may not be governed by the standard Kosterlitz-Thouless theory in two dimensions. Future superfluid density measurements on FeSe films with different thicknesses could help clarify this issue.

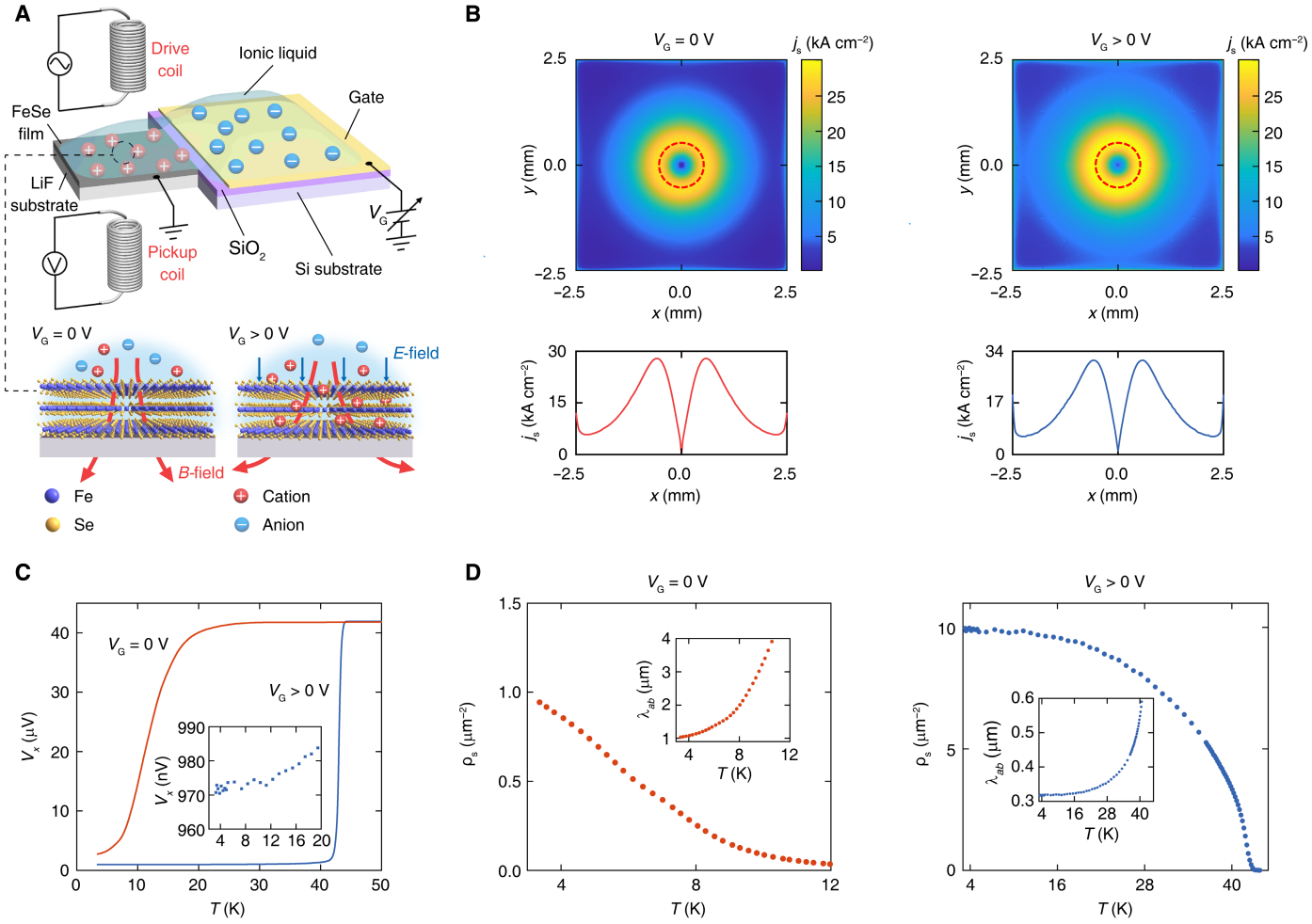

Fig. 1. Operando superfluid density measurements on the ion-gated FeSe film. (**A**) Schematic of a typical ILG device and the TCMI measurement scheme. The ILG device consists of an FeSe film and a gate electrode, with the ionic liquid DEME-TFSI covered. A positive gate voltage (V_G) is applied between the gate electrode and the film to induce the electrochemical protonation. A drive coil and a pickup coil are mounted on opposite sides of the ILG device for in situ measurements of the diamagnetic response of the sample. Under a positive V_G, the cations in the DEME-TFSI will enter the FeSe film, resulting in an enhancement of the superfluid density. Consequently, the diamagnetic response becomes stronger, from which the evolution of superfluid density with ILG can be extracted. (**B**) Top view of the magnitude of the induced screening current density, j_s, for the pristine state with $T_c \approx 11$ K (left column) and the gated state with $T_c \approx 43$ K (right column), calculated using the FWC method (*29*). The red dashed line denotes the position of the drive coil. The bottom panels show the cuts at $y = 0$. (**C**) Temperature dependence of the real component of the pickup coil voltage, V_x, for the pristine state (red line) and the gated state (blue line). The sudden drop in V_x around T_c reflects the strong diamagnetism of the superconducting state. Inset: Zoom-in of the V_x versus T curve for the gated state. The absence of the diamagnetic transition near the original T_c of 11 K indicates bulk modulation of the superconductivity by ILG (*28*). (**D**) Temperature-dependent superfluid density, $\rho_s(T)$, for the pristine state (left) and the gated state (right), extracted from the data in (C). The inset shows the temperature-dependent in-plane magnetic penetration depth, $\lambda_{ab}(T)$.

We noticed that the $T_c \propto \rho_{s0}^{0.5}$ relation was also observed near the critical doping where superconductivity vanishes (*20*, *43*) and was attributed to the critical quantum phase fluctuations (*36*, *44*, *45*). Besides, a similar scaling relation is found by our 2D-YSYK modeling of a quantum critical metal with fermion-scalar Yukawa couplings and potential disorder (fig. S16B). Although further studies are needed to determine the mechanism responsible for the $T_c(\rho_{s0})$ scaling observed here, the strong correlation between T_c and ρ_{s0} demonstrates that phase rigidity plays a dominant role in determining T_c of ion-gated FeSe, in contrast to the standard BCS paradigm where T_c is bounded by the temperature at which Cooper pairs form. This is corroborated by large ratios of $(T_c/T_F, \Delta_{min}/E_F) \approx (0.11, 0.23)$ for samples with $T_c > 39$ K ($E_F = k_B T_F$ is the effective Fermi energy derived from ρ_{s0}), indicating that ion-gated FeSe locates in the BCS–Bose-Einstein condensation (BEC) crossover regime (*32*) (Fig. 2D).

Scaling of the superfluid density with *T*-linear resistivity coefficient

By displaying the systematic ρ_s data in the phase diagram with varying electron doping and temperature, we are able to trace the evolution of the superconducting condensate with the normal-state transport (Fig. 3A). Intriguingly, we find that the magnitude of the superfluid density and the strength of the T-linear resistivity are synchronously enhanced with electron doping, which is accompanied by the similar increasing trends for T_c (see the gray circles and

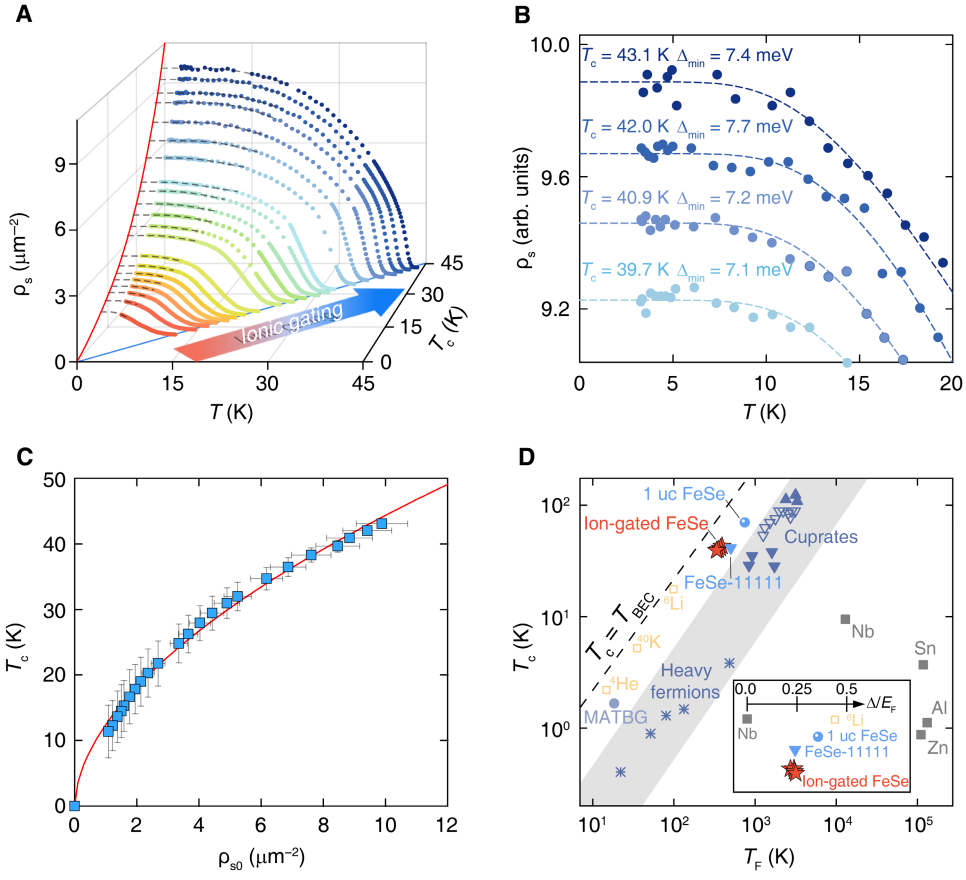

Fig. 2. Evolution of the superfluid density in the ion-gated FeSe film. (**A**) Temperature-dependent superfluid density, $\rho_s(T)$, for the ion-gated FeSe film with T_c systematically tuned from ~11 to 43 K. The dashed lines are the nodeless-gap fits to the first 10% drop in $\rho_s(T) / \rho_s(T \to 0)$, as depicted in the expanded view of the ρ_s data at low temperatures in (**B**). arb. units, arbitrary units. (**C**) Dependence of T_c on the zero-temperature superfluid density, $\rho_{s0} \equiv \rho_s(T \to 0)$, where ρ_{s0} is determined from the nodeless-gap fit. The blue squares represent the experimental data; the red solid line is the fit to $T_c = \gamma\rho_{s0}^{0.55}$, where γ is the fit parameter. (**D**) Uemura plot: T_c versus Fermi temperature, T_F, for various superconductors (*59*). The ion-gated FeSe with $T_c > 39$ K, as well as other FeSe-based superconductors, i.e., monolayer FeSe on $SrTiO_3$ substrate [1 unit cell (uc) FeSe] and $(Li_{0.8}Fe_{0.2})$OHFeSe (FeSe-11111) are located closer to the BEC limit for 3D bosonic gas ($T_c = 0.218T_F$, the dashed line) than cuprate and heavy-fermion superconductors (the shaded region). The large ratio of $\Delta/E_F \approx 0.23$ for ion-gated FeSe also indicates that it lies in the BCS-BEC crossover regime (see the inset). T_F and E_F are obtained from ρ_{s0} using the formula given in (*32*), i.e., $E_F = k_B T_F = \frac{\pi\hbar^2 d}{\mu_0 e^2}\rho_{s0}$, where d is the interlayer distance. The values of Δ are obtained from the nodeless-gap fits in (B).

gray squares) and the upper bound temperature of T-linear resistivity (T_1 defined in the inset of fig. S8). These observations provide strong evidence that the formation of superfluid condensation is linked with the strange-metal normal state, which is compatible with the scenario recently proposed in overdoped cuprates that superfluid condensation originates from incoherent carriers contributing to the strange-metal transport (*12*, *22*). To the best of our knowledge, such a visualized description of the interplay between unconventional superconductivity and the strange metallicity has not been established before.

Figure 3B shows both ρ_{s0} and $A_1^{\square}$ as a function of electron doping for the ion-gated FeSe film, where $A_1^{\square}$ is the T-linear resistivity coefficient normalized by the distance between adjacent superconducting layers. Notably, ρ_{s0} tracks $A_1^{\square}$ closely for all gated states, which unambiguously points to a linear correlation between ρ_{s0} and $A_1^{\square}$, i.e., $\rho_{s0} = \alpha\widetilde{A}_1^{\square}$ with $\alpha = 0.43 \pm 0.02$ μm^{-2} ohms^{-1} K (Fig. 3C). Here, a constant has been subtracted from $A_1^{\square}$, namely, $\widetilde{A}_1^{\square} = A_1^{\square} - A_0$, where $A_0 = 17.5$ ohms K^{-1} represents the nonzero extrapolation of A_1 to $\rho_{s0} = 0$ μm^{-2} or $T_c = 0$ K (*5*). With the error bars taken into account, the linear relationship is the best fit to the ρ_{s0} versus $A_1^{\square}$ data (Supplementary Text 6 and fig. S10). Note that the Drude model provides $A_1^{\square} \propto \Gamma m^*/n$, where Γ is the scattering rate for the T-linear resistivity and n is the carrier density. Considering that the change in the residual resistivity ρ_0 with doping can provide a reasonable estimate of the change in n (*46*), the change in $(A_1^{\square})^* = A_1^{\square}\rho_0(0)/\rho_0(p)$ [$\rho_0(0)$ and $\rho_0(p)$ are the residual resistivities of the pristine state and the gated state, respectively] could reflect the variation of the scattering strength. As shown in fig. S11, the relative change in ρ_{s0} (≈ 433%) is comparable with the relative change in $(A_1^{\square})^*$ (≈ 317%), suggesting that the growth rates of the superfluid density and the scattering strength under ILG are almost consistent.

To figure out to what extent the linear scaling of ion-gated FeSe is applied to other superconducting materials, we collect the ρ_{s0} and $A_1^{\square}$ data from previous reports (see the original data in fig. S12). Systematic $A_1^{\square}$ data of electron-doped cuprate $La_{2-x}Ce_xCuO_4$ (LCCO) have been obtained on composition-spread films (*3*), but corresponding ρ_{s0} data are lacking due to the difficulty of accurately characterizing the local superfluid density. The calculated upper bound

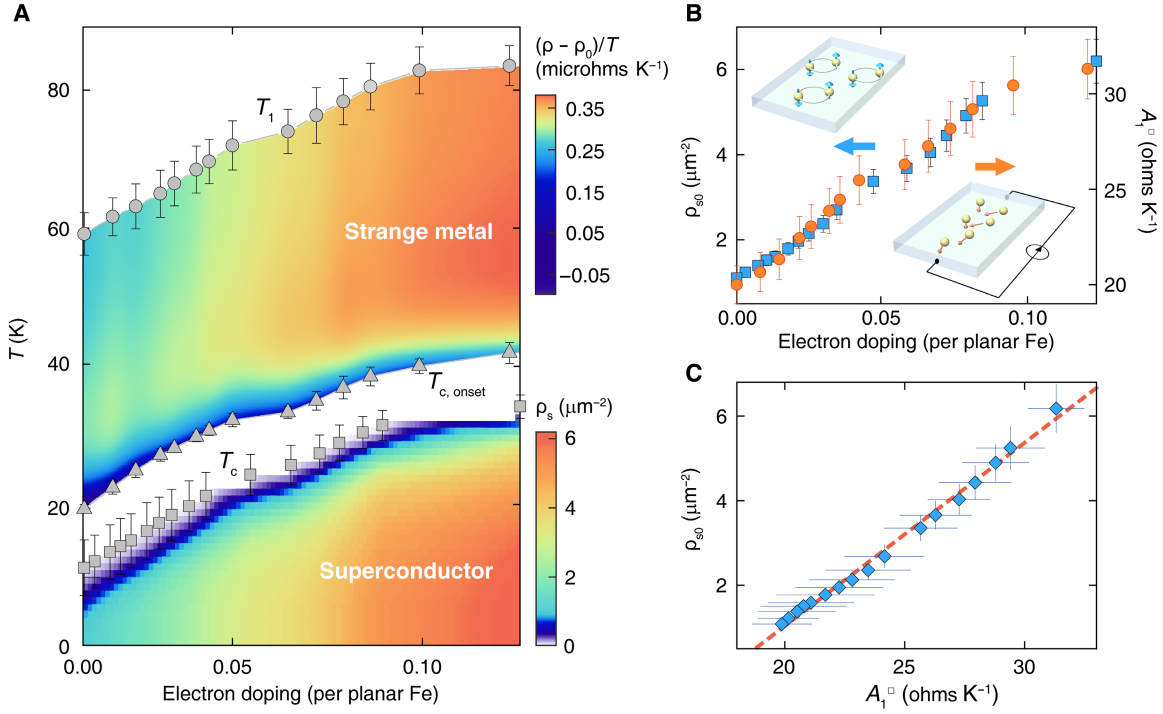

Fig. 3. Correlation between unconventional superconductivity and the strange metallicity in the ion-gated FeSe film. (**A**) Synchronized evolution of the strange-metal phase and the superfluid condensate with ILG. The strength of the strange-metal resistivity, $(\rho - \rho_0)/T$, and the magnitude of the superfluid density, $\rho_s \equiv \lambda_{ab}^{-2}$, versus temperature T and election doping level are shown by the contour plot. The gray circles, gray triangles, and gray squares represent the upper bound temperature of T-linear resistivity (T_1), the onset temperature of superconducting transition ($T_{c,onset}$), and T_c, respectively. The definitions of T_1 and $T_{c,onset}$ can be found in the inset of fig. S8. It is shown that the strange-metal phase [characterized by $(\rho - \rho_0)/T$ and T_1] and the superfluid condensate (characterized by ρ_s and T_c) change synchronously with doping. Here, ρ_0 is the residual resistivity obtained by fitting the resistivity at low temperatures with the function $\rho = \rho_0 + A_1 T$. The normal state data are extracted from fig. S9. The doping levels are extracted from the T_c versus doping relation in (*5*). (**B**) Zero-temperature superfluid density, ρ_{s0}, (blue squares) and the T-linear coefficient per Fe-Se layer, $A_1^{\square}$, (red circles) versus electron doping in the ion-gated FeSe film. Here, $A_1^{\square} = A_1/d_{Fe\text{-}Se}$, where $d_{Fe\text{-}Se}$ is the distance between adjacent Fe-Se layers. Evidently, ρ_{s0} tracks $A_1^{\square}$ closely with electron doping, demonstrating a direct link between the formation of the superfluid in the ground state and the strange-metal behavior in the normal state. (**C**) ρ_{s0} as a function of $A_1^{\square}$ in the ion-gated FeSe film. Raw data can be found in table S1.

of ρ_{s0} and measured $A_1^{\square}$ of magic-angle graphene follow the similar trend as doping varies (*6*, *47*), but systematic superfluid measurements are required to obtain a quantitative relation. In spite of large error bars, the data of iron-pnictide superconductors BFCA reside in the linear trend. For overdoped Tl2201, ρ_{s0} and $A_1^{\square}$ were found to decrease in tandem with the increase in hole doping, as pointed out by Phillips *et al.* (*22*), which is similar to our finding and implies a linear relation despite the relatively scarce data points. For overdoped LSCO, although the strong correlation between ρ_{s0} and $A_1^{\square}$ still persists, a quantitative relationship cannot be pinned down due to the large uncertainty of the $A_1^{\square}$ data (fig. S13). The data points of $A_1^{\square}$ and ρ_{s0} are well fitted by a linear relation within the error bar, particularly in the regime of $T_c < 12$ K. To summarize, we plot the $\rho_{s0}/(\rho_{s0})^{max}$ versus $\widetilde{A}_1^{\square}/(\widetilde{A}_1^{\square})^{max}$ relationship in Fig. 4A (the superscript max refers to the maximum values in the literature), which suggests a linear scaling behavior that captures the common relation between ρ_{s0} and $A_1^{\square}$ among different superconducting systems.

DISCUSSION

The similarity of ion-gated FeSe and overdoped cuprates revealed by the ρ_{s0} versus $A_1^{\square}$ relation is unexpected because they are distinct in many aspects. In overdoped cuprates, the normal-state carrier density exhibits an anticorrelation with ρ_{s0} as the hole doping varies (*12*, *20*), whereas in FeSe, the ILG gives rise to the enhancement in ρ_{s0}, accompanied by an increase in the electron density and a decrease in the hole density (Supplementary Text 2 and fig. S3). FeSe's nodeless gap [see, e.g., (*32*) and Fig. 2B] also indicates that it differs from the cuprates in the pairing symmetry. Hence, the universal scaling shown in Fig. 4A indicates a fundamental link between superconducting condensation and the strange metallicity in unconventional superconductors.

It has been suggested that the strong electron pairing is always linked with the large $A_1^{\square}$ in the strange-metal normal state (*2*, *15*). Within this framework, the impurity scattering due to disorder is expected to reduce the pairing interaction, thereby reducing $A_1^{\square}$. Meanwhile, it will suppress the long-range phase coherence and/or induce pair breaking, leading to the decrease in ρ_{s0}. Therefore, the effects of disorder may play an important role in the correlation between ρ_{s0} and $A_1^{\square}$. For the ion-gated state with $T_c \approx 40$ K, the electronic mean free path (l = 3.6 nm) deduced from the in situ Seebeck and Hall measurements (*48*) is comparable to the zero-temperature in-plane coherence length [$\xi_{ab}(0) = 2.3$ nm] derived from the upper critical field (Supplementary Text 7 and fig. S14), pointing to the relatively dirty nature of FeSe films. For overdoped cuprates, recent studies also reveal the impact of the disorder on

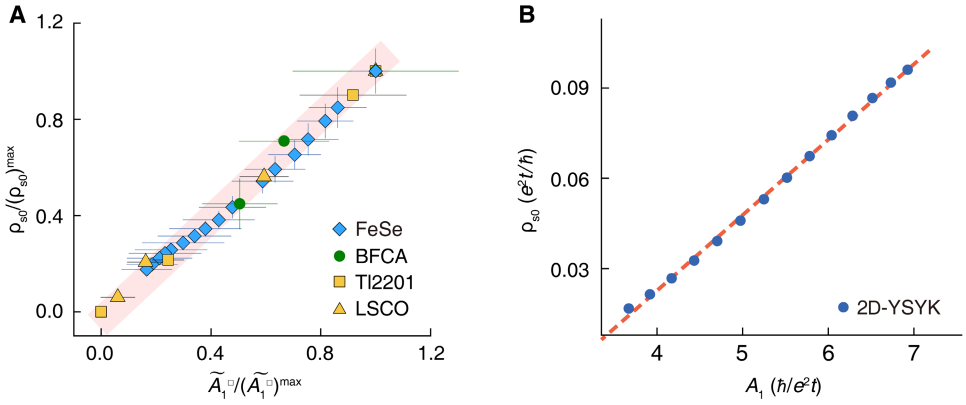

Fig. 4. Scaling of the zero-temperature superfluid density and the *T*-linear resistivity coefficient for unconventional superconductors. (**A**) Scaling of ρ_{s0} with $\widetilde{A}_1^{\square}$ for different superconducting systems, where ρ_{s0} and $\widetilde{A}_1^{\square}$ are normalized by their respective maximum values in the literature. Here, a constant has been subtracted from $A_1^{\square}$, namely, $\widetilde{A}_1^{\square} = A_1^{\square} - A_0$, where A_0 represents the nonzero extrapolation of A_1 to $T_c = 0$ K (*5*). Data for $Ba(Fe_{1-x}Co_x)_2As_2$ (BFCA) are extracted from (*3*, *34*). Data for $Tl_2Ba_2CuO_{6+\delta}$ (Tl2201) are obtained from (*22*) and references therein. Data for heavily overdoped $La_{2-x}Sr_xCuO_4$ (LSCO; $T_c \leq 12$ K) are extracted from (*5*, *20*). The error bars are reproduced from published data. The red shading is a guide to the eye. (**B**) ρ_{s0} versus A_1 relation calculated on the basis of the 2D-YSYK model (Materials and Methods and Supplementary Text 8), where $\hbar$ is the reduced Planck's constant and t is the fermion hopping.

both the normal-state transport and the superconducting properties [see, e.g., (*49*, *50*)].

On the other hand, it has been believed that the *T*-linear resistivity, as well as the unconventional superconductivity, could stem from the quantum fluctuations near a QCP (*51*–*53*). For FeSe, applying a small pressure can induce the emergence of a spin density wave order (*54*), suggesting that FeSe is in the proximity of a magnetically ordered state, and the increase in T_c by ILG may also be associated with an approach to a putative magnetic QCP. As the system moves away from the QCP, strange-metal scattering induced by quantum critical fluctuation is presumably reduced, thus decreasing $A_1^{\square}$. Simultaneously, the pairing interaction relative to impurity scattering effects weakens further from the QCP, yielding the enhanced pair breaking and decreased ρ_{s0}. Consequently, we expect that the quantum criticality is another key ingredient governing the observed correlation between ρ_{s0} and $A_1^{\square}$.

To gain deeper theoretical insight into the observed correlation between ρ_{s0} versus A_1, we turn to the 2D-YSYK model (*25*–*27*), a theoretical framework recently developed to capture universal features of strange-metal behavior and unconventional superconductivity near a QCP in the presence of quenched spatial disorder. In this model, fermions near a Fermi surface couple to nearly critical bosonic modes through spatially random Yukawa couplings (Materials and Methods), giving rise to a strange-metal phase characterized by linear-in-*T* resistivity and a superconducting instability depending on the interaction strength. Notably, by varying the renormalized boson mass *M* and the potential disorder stimulatingly (Supplementary Text 8), a linear ρ_{s0} versus A_1 relation is reproduced (Fig. 4B). Here, tuning the renormalized boson mass *M* effectively controls the distance to the putative QCP (*26*)—analogous to the basic effect of doping or gating in experiments. Besides, such a choice of model parameters is consistent with the fact that doping or gating also alters the disorder strength. Disorder is a strongly relevant perturbation to clean quantum criticality, which can explain the applicability of the 2D-YSYK theory to relatively clean samples (*26*, *55*). The agreement between the theoretical calculations and the experimental data thus suggests the universal scaling we observe may emerge from a fundamental mechanism involving the cooperative effects of quantum critical fluctuations and spatial disorder.

In addition, a nonzero extrapolation of $A_1^{\square}$ to $\rho_{s0} = 0\ \mu m^{-2}$ or $T_c = 0$ K is seemingly ubiquitous in overdoped cuprates including LSCO and Bi2201 (*13*), which is witnessed from the difference between the boundaries of superconducting dome (p_{sc}) and the strange-metal phase (p_{sm}) in the *T* versus doping phase diagram, as depicted in fig. S17. This may originate from the suppression of superconductivity between p_{sc} and p_{sm} due to pair breaking (*56*) or the presence of competing orders (*57*). Besides, it was suggested that the multiorbital effect in iron-based superconductors, which involves orbital-dependent quasiparticle spectral weights in the normal state and orbital-selective pairing in the superconducting state (*58*), could contribute to the residual $A_1^{\square}$ (*5*). Whether these scenarios could account for the residual $A_1^{\square}$ remains to be investigated.

MATERIALS AND METHODS

Experiment

Device fabrication

An FeSe/LiF film with a size of 5 mm by 5 mm is placed next to a Si substrate covered by the SiO_2 insulating layer. A gate electrode with a size of 10 mm by 7 mm is fabricated on the SiO_2 layer by depositing Au/Ti (50 nm/5 nm) with electron beam evaporation. Electrical contacts are made by indium (In) soldering on the side of the FeSe film and a corner of the gate electrode. The ionic liquid DEME-TFSI is covered by a 6-μm-thick Kapton foil to confine its coverage on the sample and the gate electrode (fig. S4A).

In situ TCMI measurements

During the ILG, the ILG device is mounted inside a sapphire block of the TCMI apparatus (fig. S4B). A drive coil and a pickup coil are sealed in the sapphire block with epoxy and aligned axially with the center of the FeSe film. The two coils are the same in size: The number of turns is 300, the inner diameter is 0.5 mm, the outer diameter is 1.3 mm, and the length is 1.6 mm. The pickup coil is pressed against the backside of the LiF substrate, whereas the drive coil is about 0.4 mm away from the surface of the FeSe film. A plastic

electric board is fastened on the sapphire block to provide a platform for wiring. To reduce noise and interference, coils are connected to coaxial cables. The apparatus is thermally connected to the 3-K platform of a Montana Instruments cryocooler. A Lakeshore thermometer is mounted inside the sapphire block to measure the sample temperature. A Keithley 2450 source meter is used to apply the gate voltage and monitor the leakage current. A Stanford Research SR830 lock-in amplifier is used to supply the alternating current to the drive coil. The current amplitude is 0.2 mA, and the frequency is 50 kHz, which is in the linear-response regime. The induced pickup coil voltage, $V = V_x + iV_y$, is probed by the same lock-in amplifier with a reference phase of 90°.

A complete experiment includes a set of sequences, each of which involves (i) warming up to a target temperature (T_G) under a positive gate voltage (V_G), (ii) staying at the target temperature for a given period of time (t_G), and (iii) cooling down to measure the induced pickup coil voltage.

Extracting the magnetic penetration depth using the FWC method

When the films enter the Meissner state, two types of currents in the system will contribute to V_x. One is the alternating current applied to the drive coil, whose contribution can be calculated with the coil parameters on the basis of classical electrodynamics. The other is the screening current induced in the superconducting film, which is related to λ_{ab} through (*29*)

$$\mathbf{j}_s(\mathbf{r}) + \frac{\sinh(d/\lambda_{ab})}{4\pi\lambda_{ab}} \int_\Omega d^2\mathbf{r}' \frac{\mathbf{j}_s(\mathbf{r}')}{|\mathbf{r}-\mathbf{r}'|} = -\frac{1}{\mu_0 {\lambda_{ab}}^2} \mathbf{A}_d(\mathbf{r}) \quad (1)$$

where $\mathbf{j}_s$ is the screening current density, Ω is the projection of the film on the x-y plane (film surface), $\mathbf{r} = \hat{\mathbf{x}}x + \hat{\mathbf{y}}y$, d is the film thickness, $\mu_0 = 4\pi \times 10^{-7}$ N A^{-2} is the vacuum permeability, and $\mathbf{A}_d$ is the vector potential generated by the drive current. Using the FWC algorithm, Eq. 1 can be accurately solved and $\mathbf{j}_s$ is obtained (Fig. 1B). Then, the real component of the pickup coil voltage, V_x, can be calculated by integrating the vector potential of both the drive and screening currents around each loop of the pickup coil. Last, the absolute value of the superfluid density, $\rho_s = \lambda_{ab}^{-2}$, can be extracted by interpolating the measured V_x into the calculated relation between V_x and ρ_s (fig. S5). More details about this procedure can be found in (*29*).

Theory

2D-YSYK model

This section will consider the 2D-YSYK model (*25*–*27*) with the potential disorder v and the spatially random Yukawa coupling g'. We start with the imaginary time action

$$\begin{aligned} S = &\int d\tau \sum_{\mathbf{k},\sigma=\pm1} \sum_{i=1}^{N} \psi^\dagger_{i\mathbf{k}\sigma}(\tau)\left[\partial_\tau + \epsilon(\mathbf{k})\right]\psi_{i\mathbf{k}\sigma}(\tau) \\ &+ \frac{1}{2}\int d\tau \sum_{\mathbf{q}} \sum_{i=1}^{N} \phi_{i\mathbf{q}}(\tau)\left[-\partial_\tau^2 + \omega^2(\mathbf{q})\right]\phi_{i,-\mathbf{q}}(\tau) \\ &+ \int d\tau d^2r \sum_{i,j=1}^{N} \sum_{\sigma=\pm1} \frac{v_{ij}(\mathbf{r})}{\sqrt{N}} \psi^\dagger_{i\sigma}(\mathbf{r},\tau)\psi_{j\sigma}(\mathbf{r},\tau) \\ &+ \int d\tau d^2r \sum_{i,j,l=1}^{N} \sum_{\sigma=\pm1} \frac{g'_{ijl}(\mathbf{r})}{N} \psi^\dagger_i(\mathbf{r},\tau)\psi_j(\mathbf{r},\tau)\phi_l(\mathbf{r},\tau) \end{aligned} \quad (2)$$

where the potential disorder v_{ij} and interaction disorder g'_{ijl} satisfy

$$\begin{aligned} &\overline{v_{ij}(\mathbf{r})} = 0, \quad \overline{v^*_{ij}(\mathbf{r})v_{i'j'}(\mathbf{r}')} = v^2\delta(\mathbf{r}-\mathbf{r}')\delta_{ii'}\delta_{jj'}, \\ &\overline{g'_{ijl}(\mathbf{r})} = 0, \quad \overline{g'^*_{ijl}(\mathbf{r})g'_{i'j'l'}(\mathbf{r}')} = g'^2\delta(\mathbf{r}-\mathbf{r}')\delta_{ii'}\delta_{jj'}\delta_{ll'} \end{aligned} \quad (3)$$

The lattice dispersion is chosen as

$$\begin{aligned} \epsilon(\mathbf{k}) &= -2t(\cos k_z + \cos k_y) - \mu, \\ \omega^2(\mathbf{q}) &= m_b^2 + 2J(2 - \cos q_x - \cos q_y) \end{aligned} \quad (4)$$

where t is the fermion hopping, μ is the chemical potential, m_b is the bare boson mass, and J determines the boson dispersion. Details about the calculations of the resistivity and the superfluid density in the 2D-YSYK model can be found in Supplementary Text 8.

Supplementary Materials

This PDF file includes:

Supplementary Texts 1 to 8
Figs. S1 to S17
Table S1
References

REFERENCES AND NOTES

1. R. A. Cooper, Y. Wang, B. Vignolle, O. J. Lipscombe, S. M. Hayden, Y. Tanabe, T. Adachi, Y. Koike, M. Nohara, H. Takagi, C. Proust, N. E. Hussey, Anomalous criticality in the electrical resistivity of $La_{2-x}Sr_xCuO_4$. *Science* **323**, 603–607 (2009).
2. K. Jin, N. P. Butch, K. Kirshenbaum, J. Paglione, R. L. Greene, Link between spin fluctuations and electron pairing in copper oxide superconductors. *Nature* **476**, 73–75 (2011).
3. J. Yuan, Q. Chen, K. Jiang, Z. Feng, Z. Lin, H. Yu, G. He, J. Zhang, X. Jiang, X. Zhang, Y. Shi, Y. Zhang, M. Qin, Z. G. Cheng, N. Tamura, Y.-f. Yang, T. Xiang, J. Hu, I. Takeuchi, K. Jin, Z. Zhao, Scaling of the strange-metal scattering in unconventional superconductors. *Nature* **602**, 431–436 (2022).
4. S. Licciardello, J. Buhot, J. Lu, J. Ayres, S. Kasahara, Y. Matsuda, T. Shibauchi, N. E. Hussey, Electrical resistivity across a nematic quantum critical point. *Nature* **567**, 213–217 (2019).
5. X. Jiang, M. Qin, X. Wei, L. Xu, J. Ke, H. Zhu, R. Zhang, Z. Zhao, Q. Liang, Z. Wei, Z. Lin, Z. Feng, F. Chen, P. Xiong, J. Yuan, B. Zhu, Y. Li, C. Xi, Z. Wang, M. Yang, J. Wang, T. Xiang, J. Hu, K. Jiang, Q. Chen, K. Jin, Z. Zhao, Interplay between superconductivity and the strange-metal state in FeSe. *Nat. Phys.* **19**, 365–371 (2023).
6. Y. Cao, D. Chowdhury, D. Rodan-Legrain, O. Rubies-Bigorda, K. Watanabe, T. Taniguchi, T. Senthil, P. Jarillo-Herrero, Strange metal in magic-angle graphene with near Planckian dissipation. *Phys. Rev. Lett.* **124**, 076801 (2020).
7. K. Lee, B. Y. Wang, M. Osada, B. H. Goodge, T. C. Wang, Y. Lee, S. Harvey, W. J. Kim, Y. Yu, C. Murthy, S. Raghu, L. F. Kourkoutis, H. Y. Hwang, Linear-in-temperature resistivity for optimally superconducting (Nd,Sr)NiO_2. *Nature* **619**, 288–292 (2023).
8. Y. Zhang, D. Su, Y. Huang, Z. Shan, H. Sun, M. Huo, K. Ye, J. Zhang, Z. Yang, Y. Xu, Y. Su, R. Li, M. Smidman, M. Wang, L. Jiao, H. Yuan, High-temperature superconductivity with zero resistance and strange-metal behaviour in $La_3Ni_2O_{7-\delta}$. *Nat. Phys.* **20**, 1269–1273 (2024).
9. Y. Zhu, D. Peng, E. Zhang, B. Pan, X. Chen, L. Chen, H. Ren, F. Liu, Y. Hao, N. Li, Z. Xing, F. Lan, J. Han, J. Wang, D. Jia, H. Wo, Y. Gu, Y. Gu, L. Ji, W. Wang, H. Gou, Y. Shen, T. Ying, X. Chen, W. Yang, H. Cao, C. Zheng, Q. Zeng, J.-g. Guo, J. Zhao, Superconductivity in pressurized trilayer $La_4Ni_3O_{10-\delta}$ single crystals. *Nature* **631**, 531–536 (2024).
10. L. Chen, D. T. Lowder, E. Bakali, A. M. Andrews, W. Schrenk, M. Waas, R. Svagera, G. Eguchi, L. Prochaska, Y. Wang, C. Setty, S. Sur, Q. Si, S. Paschen, D. Natelson, Shot noise in a strange metal. *Science* **382**, 907–911 (2023).
11. B. Keimer, S. A. Kivelson, M. R. Norman, S. Uchida, J. Zaanen, From quantum matter to high-temperature superconductivity in copper oxides. *Nature* **518**, 179–186 (2015).
12. C. Putzke, S. Benhabib, W. Tabis, J. Ayres, Z. Wang, L. Malone, S. Licciardello, J. Lu, T. Kondo, T. Takeuchi, N. E. Hussey, J. R. Cooper, A. Carrington, Reduced Hall carrier density in the overdoped strange metal regime of cuprate superconductors. *Nat. Phys.* **17**, 826–831 (2021).
13. J. Ayres, M. Berben, M. Culo, Y. T. Hsu, E. van Heumen, Y. Huang, J. Zaanen, T. Kondo, T. Takeuchi, J. R. Cooper, C. Putzke, S. Friedemann, A. Carrington, N. E. Hussey, Incoherent transport across the strange-metal regime of overdoped cuprates. *Nature* **595**, 661–666 (2021).
14. R. L. Greene, P. R. Mandal, N. R. Poniatowski, T. Sarkar, The strange metal state of the electron-doped cuprates. *Annu. Rev. Condens. Matter Phys.* **11**, 213–229 (2020).

15. L. Taillefer, Scattering and pairing in cuprate superconductors. *Annu. Rev. Condens. Matter Phys.* **1**, 51–70 (2010).
16. Y. J. Uemura, G. M. Luke, B. J. Sternlieb, J. H. Brewer, J. F. Carolan, W. N. Hardy, R. Kadono, J. R. Kempton, R. F. Kiefl, S. R. Kreitzman, P. Mulhern, T. M. Riseman, D. L. Williams, B. X. Yang, S. Uchida, H. Takagi, J. Gopalakrishnan, A. W. Sleight, M. A. Subramanian, C. L. Chien, M. Z. Cieplak, G. Xiao, V. Y. Lee, B. W. Statt, C. E. Stronach, W. J. Kossler, X. H. Yu, Universal correlations between T_c and n_s/m^* (carrier density over effective mass) in high-T_c cuprate superconductors. *Phys. Rev. Lett.* **62**, 2317–2320 (1989).
17. Y. J. Uemura, L. P. Le, G. M. Luke, B. J. Sternlieb, W. D. Wu, J. H. Brewer, T. M. Riseman, C. L. Seaman, M. B. Maple, M. Ishikawa, D. G. Hinks, J. D. Jorgensen, G. Saito, H. Yamochi, Basic similarities among cuprate, bismuthate, organic, Chevrel-phase, and heavy-fermion superconductors shown by penetration-depth measurements. *Phys. Rev. Lett.* **66**, 2665–2668 (1991).
18. Y. J. Uemura, A. Keren, L. P. Le, G. M. Luke, W. D. Wu, Y. Kubo, T. Manako, Y. Shimakawa, M. Subramanian, J. L. Cobb, J. T. Markert, Magnetic-field penetration depth in $Tl_2Ba_2CuO_{6+\delta}$ in the overdoped regime. *Nature* **364**, 605–607 (1993).
19. C. Niedermayer, C. Bernhard, U. Binninger, J. L. Tallon, E. J. Ansaldo, J. I. Budnick, Muon spin rotation study of the correlation between T_c and n_s/m^* in $Tl_2Ba_2CuO_{6+\delta}$. *Phys. Rev. Lett.* **71**, 1764 (1993).
20. I. Božović, X. He, J. Wu, A. T. Bollinger, Dependence of the critical temperature in overdoped copper oxides on superfluid density. *Nature* **536**, 309–311 (2016).
21. V. J. Emery, S. A. Kivelson, Importance of phase fluctuations in superconductors with small superfluid density. *Nature* **374**, 434–437 (1995).
22. P. W. Phillips, N. E. Hussey, P. Abbamonte, Stranger than metals. *Science* **377**, eabh4273 (2022).
23. C. Leighton, Electrolyte-based ionic control of functional oxides. *Nat. Mater.* **18**, 13–18 (2019).
24. B. Lei, J. H. Cui, Z. J. Xiang, C. Shang, N. Z. Wang, G. J. Ye, X. G. Luo, T. Wu, Z. Sun, X. H. Chen, Evolution of high-temperature superconductivity from a low-T_c phase tuned by carrier concentration in FeSe thin flakes. *Phys. Rev. Lett.* **116**, 077002 (2016).
25. A. A. Patel, H. Guo, I. Esterlis, S. Sachdev, Universal theory of strange metals from spatially random interactions. *Science* **381**, 790–793 (2023).
26. C. Li, D. Valentinis, A. A. Patel, H. Guo, J. Schmalian, S. Sachdev, I. Esterlis, Strange metal and superconductor in the two-dimensional Yukawa-Sachdev-Ye-Kitaev model. *Phys. Rev. Lett.* **133**, 186502 (2024).
27. A. Hardy, O. Parcollet, A. Georges, A. A. Patel, Enhanced strange metallicity due to Hubbard-*U* Coulomb repulsion. *Phys. Rev. Lett.* **134**, 036502 (2025).
28. M. Qin, R. Zhang, Z. Lin, Z. Feng, X. Wei, S. Blanco Alvarez, C. Dong, A. V. Silhanek, B. Zhu, J. Yuan, Q. Qin, K. Jin, In situ magnetic measurements of ionic-liquid-gated superconducting films. *J. Supercond. Nov. Magn.* **33**, 159–163 (2020).
29. R. Zhang, M. Qin, L. Zhang, L. You, C. Dong, P. Sha, Q. Chen, J. Yuan, K. Jin, Determining the absolute value of magnetic penetration depth in small-sized superconducting films. *Supercond. Sci. Technol.* **34**, 085022 (2021).
30. K. Hashimoto, T. Shibauchi, S. Kasahara, K. Ikada, S. Tonegawa, T. Kato, R. Okazaki, C. J. van der Beek, M. Konczykowski, H. Takeya, K. Hirata, T. Terashima, Y. Matsuda, Microwave surface-impedance measurements of the magnetic penetration depth in single crystal $Ba_{1-x}K_xFe_2As_2$ superconductors: Evidence for a disorder-dependent superfluid density. *Phys. Rev. Lett.* **102**, 207001 (2009).
31. H. T. Lin, S. L. Wu, J. W. Wang, T. J. Chen, M. J. Wang, J. C. Chen, M. K. Wu, C. C. Chi, Determination of the London penetration depth of $FeSe_{0.3}Te_{0.7}$ thin films by scanning SQUID microscope. *Supercond. Sci. Technol.* **28**, 085006 (2015).
32. T. Shibauchi, T. Hanaguri, Y. Matsuda, Exotic superconducting states in FeSe-based materials. *J. Physical Soc. Japan* **89**, 102002 (2020).
33. R. Valdés Aguilar, L. S. Bilbro, S. Lee, C. W. Bark, J. Jiang, J. D. Weiss, E. E. Hellstrom, D. C. Larbalestier, C. B. Eom, N. P. Armitage, Pair-breaking effects and coherence peak in the terahertz conductivity of superconducting $BaFe_{2-2x}Co_{2x}As_2$ thin films. *Phys. Rev. B* **82**, 180514(R) (2010).
34. T. J. Williams, A. A. Aczel, E. Baggio-Saitovitch, S. L. Bud'ko, P. C. Canfield, J. P. Carlo, T. Goko, H. Kageyama, A. Kitada, J. Munevar, N. Ni, S. R. Saha, K. Kirschenbaum, J. Paglione, D. R. Sanchez-Candela, Y. J. Uemura, G. M. Luke, Superfluid density and field-induced magnetism in $Ba(Fe_{1-x}Co_x)_2As_2$ and $Sr(Fe_{1-x}Co_x)As_2$ measured with muon spin relaxation. *Phys. Rev. B* **82**, 094512 (2010).
35. Y. Zuev, M. S. Kim, T. R. Lemberger, Correlation between superfluid density and T_c of underdoped $YBa_2Cu_3O_{6+x}$ near the superconductor-insulator transition. *Phys. Rev. Lett.* **95**, 137002 (2005).
36. I. Hetel, T. R. Lemberger, M. Randeria, Quantum critical behaviour in the superfluid density of strongly underdoped ultrathin copper oxide films. *Nat. Phys.* **3**, 700–702 (2007).
37. S. V. Dordevic, C. C. Homes, Superfluid density in overdoped cuprates: Thin films versus bulk samples. *Phys. Rev. B* **105**, 214514 (2022).
38. Z.-X. Li, S. A. Kivelson, D.-H. Lee, Superconductor-to-metal transition in overdoped cuprates. *NPJ Quantum Mater.* **6**, 36 (2021).
39. N. R. Lee-Hone, J. S. Dodge, D. M. Broun, Disorder and superfluid density in overdoped cuprate superconductors. *Phys. Rev. B* **96**, 024501 (2017).
40. V. G. Kogan, Strong pairbreaking in anisotropic superconductors. *Phys. Rev. B* **81**, 184528 (2010).
41. C. C. Homes, S. V. Dordevic, M. Strongin, D. A. Bonn, R. Liang, W. N. Hardy, S. Komiya, Y. Ando, H. Yu, N. Kaneko, X. Zhao, M. Greven, D. N. Basov, T. Timusk, A universal scaling relation in hightemperature superconductors. *Nature* **430**, 539–541 (2004).
42. C. C. Homes, S. V. Dordevic, T. Valla, M. Strongin, Scaling of the superfluid density in high-temperature superconductors. *Phys. Rev. B* **72**, 134517 (2005).
43. D. M. Broun, W. A. Huttema, P. J. Turner, S. Ozcan, B. Morgan, R. Liang, W. N. Hardy, D. A. Bonn, Superfluid density in a highly underdoped $YBa_2Cu_3O_{6+y}$ superconductor. *Phys. Rev. Lett.* **99**, 237003 (2007).
44. M. Franz, A. P. Iyengar, Superfluid density of strongly underdoped cuprate superconductors from a four-dimensional *XY* model. *Phys. Rev. Lett.* **96**, 047007 (2006).
45. S. Sachdev, *Quantum Phase Transitions* (Cambridge Univ. Press, 1999).
46. J. Ayres, M. Čulo, J. Buhot, B. Bernáth, S. Kasahara, Y. Matsuda, T. Shibauchi, A. Carrington, S. Friedemann, N. E. Hussey, Transport evidence for decoupled nematic and magnetic criticality in iron chalcogenides. *Commun. Phys.* **5**, 100 (2022).
47. T. Hazra, N. Verma, M. Randeria, Bounds on the superconducting transition temperature: Applications to twisted bilayer graphene and cold atoms. *Phys Rev. X* **9**, 031049 (2019).
48. X. Zhang, Z. Feng, X. Wei, Z. Lin, X. Jiang, W. Hu, Z. Wei, M. Qin, J. Xu, R. Xiong, J. Shi, J. Yuan, B. Zhu, Q. Chen, K. Jin, Enhancement of electron correlations in ion-gated FeSe film by in situ Seebeck and Hall measurements. *Phys. Rev. B* **103**, 214505 (2021).
49. J. M. Tranquada, P. M. Lozano, J. Yao, G. D. Gu, Q. Li, From nonmetal to strange metal at the stripe-percolation transition in $La_{2-x}Sr_xCuO_4$. *Phys. Rev. B* **109**, 184510 (2024).
50. S. Ye, M. Xu, H. Yan, Z.-X. Li, C. Zou, X. Li, Z. Hao, C. Yin, Y. Chen, X. Zhou, D.-H. Lee, Y. Wang, Emergent normal fluid in the superconducting ground state of overdoped cuprates. *Nat. Commun.* **15**, 4939 (2024).
51. D. J. Scalapino, A common thread: The pairing interaction for unconventional superconductors. *Rev. Mod. Phys.* **84**, 1383–1417 (2012).
52. T. Shibauchi, A. Carrington, Y. Matsuda, A quantum critical point lying beneath the superconducting dome in iron pnictides. *Annu. Rev. Condens. Matter Phys.* **5**, 113–135 (2014).
53. K. Ishida, S. Hosoi, Y. Teramoto, T. Usui, Y. Mizukami, K. Itaka, Y. Matsuda, T. Watanabe, T. Shibauchi, Divergent nematic susceptibility near the pseudogap critical point in a cuprate superconductor. *J. Phys. Soc. Jpn.* **89**, 064707 (2020).
54. J. P. Sun, K. Matsuura, G. Z. Ye, Y. Mizukami, M. Shimozawa, K. Matsubayashi, M. Yamashita, T. Watashige, S. Kasahara, Y. Matsuda, J. Q. Yan, B. C. Sales, Y. Uwatoko, J. G. Cheng, T. Shibauchi, Dome-shaped magnetic order competing with high-temperature superconductivity at high pressures in FeSe. *Nat. Commun.* **7**, 12146 (2016).
55. A. A. Patel, P. Lunts, S. Sachdev, Localization of overdamped bosonic modes and transport in strange metals. *Proc. Natl. Acad. Sci. U.S.A.* **121**, e2402052121 (2024).
56. D. Juskus, J. Ayres, R. Nicholls, N. E. Hussey, Insensitivity of T_c to the residual resistivity in high-T_c cuprates and the tale of two domes. *Front. Phys.* **12**, 1396463 (2024).
57. Q. Li, H.-Y. Huang, T. Ren, E. Weschke, L. Ju, C. Zou, S. Zhang, Q. Qiu, J. Liu, S. Ding, A. Singh, O. Prokhnenko, D.-J. Huang, I. Esterlis, Y. Wang, Y. Xie, Y. Peng, Prevailing charge order in overdoped $La_{2-x}Sr_xCuO_4$ beyond the superconducting dome. *Phys. Rev. Lett.* **131**, 116002 (2023).
58. P. O. Sprau, A. Kostin, A. Kreisel, A. E. Böhmer, V. Taufour, P. C. Canfield, S. Mukherjee, P. J. Hirschfeld, B. M. Andersen, J. C. S. Davis, Discovery of orbital-selective cooper pairing in FeSe. *Science* **357**, 75–80 (2017).
59. Y. Nakagawa, Y. Kasahara, T. Nomoto, R. Arita, T. Nojima, Y. Iwasa, Gate-controlled BCS-BEC crossover in a two-dimensional superconductor. *Science* **372**, 190–195 (2021).
60. F.-C. Hsu, J.-Y. Luo, K.-W. Yeh, T.-K. Chen, T.-W. Huang, P. M. Wu, Y.-C. Lee, Y.-L. Huang, Y.-Y. Chu, D.-C. Yan, M.-K. Wu, Superconductivity in the PbO-type structure α-FeSe. *Proc. Natl. Acad. Sci. U.S.A.* **105**, 14262–14264 (2008).
61. S. J. Turneaure, E. R. Ulm, T. R. Lemberger, Numerical modeling of a two-coil apparatus for measuring the magnetic penetration depth in superconducting films and arrays. *J. Appl. Phys.* **79**, 4221–4227 (1996).
62. J. A. Skinta, M. S. Kim, T. R. Lemberger, T. Greibe, M. Naito, Evidence for a transition in the pairing symmetry of the electron-doped cuprates $La_{2-x}Ce_xCuO_{4-y}$ and $Pr_{2-x}Ce_xCuO_{4-y}$. *Phys. Rev. Lett.* **88**, 207005 (2002).
63. P. J. Hirschfeld, N. Goldenfeld, Effect of strong scattering on the low-temperature penetration depth of a *d*-wave superconductor. *Phys. Rev. B* **48**, 4219–4222 (1993).
64. K. Mukasa, K. Ishida, S. Imajo, M. Qiu, M. Saito, K. Matsuura, Y. Sugimura, S. Liu, Y. Uezono, T. Otsuka, M. Čulo, S. Kasahara, Y. Matsuda, N. E. Hussey, T. Watanabe, K. Kindo, T. Shibauchi, Enhanced superconducting pairing strength near a pure nematic quantum critical point. *Phys. Rev. X* **13**, 011032 (2023).
65. E. E. Aldape, T. Cookmeyer, A. A. Patel, E. Altman, Solvable theory of a strange metal at the breakdown of a heavy Fermi liquid. *Phys. Rev. B* **105**, 235111 (2022).
66. X. Wang, X. Jiang, R. Zhang, Z. Zhao, X. Wei, Q. Chen, Enhancement of two dimensionality in electron-doped FeSe. *Sci. Sin. Phys. Mech. Astron.* **53**, 127415 (2023).

Acknowledgments: We would like to thank D.-H. Lee and Y. Matsuda for fruitful discussions. **Funding:** This work was supported by the National Key Research and Development Program of China grants 2021YFA0718700 and 2022YFA1603903; National Natural Science Foundation of China grants 12225412, 11927808, and 12274439; CAS Project for Young Scientists in Basic Research grant 2022YSBR-048; Key-Area Research and Development Program of Guangdong Province grant 2020B0101340002; and Beijing Nova Program of Science and Technology grant 20220484014. **Author contributions:** K.J. and Zhongxian Zhao conceived the project. M.Q. and Z.-X.L. supervised the project. M.Q. and R.Z. designed the TCMI measurement device. R.Z. and M.Q. developed the FWC method for extracting the magnetic penetration depth from the pickup coil voltage. R.Z. and M.Q. performed the ILG and the superfluid density measurements, with help from J.X., W.C., X.W., and Q.S. C.L. performed the calculations based on the 2D-YSYK model, with the guidance of S.S. Zhanyi Zhao synthesized the FeSe films. M.Q. and R.Z. analyzed the experimental data, with assistance from Z.W., X.J., J.Y., Y.L., and Q.C. T.X., Z.-X.L., and S.S. contributed to the theoretical discussions. R.Z., M.Q., C.L., S.S., Z.-X.L., and K.J. wrote the manuscript with input from all authors. **Competing interests:** The authors declare that they have no competing interests. **Data and materials availability:** All data needed to evaluate the conclusions in the paper are present in the paper and/or the Supplementary Materials.

Submitted 23 October 2024
Accepted 23 July 2025
Published 22 August 2025
10.1126/sciadv.adu0795